Preparation of Cu-doped TiO_2 via Refluxing of Alkoxide Solution and Its Photocatalytic Properties

Hiromasa Nishikiori,[1]* Takashi Sato,[1] Satoshi Kubota,[1] Nobuaki Tanaka,[1] Yuichiro Shimizu,[2] Tsuneo Fujii[1]

[1]*Department of Environmental Science and Technology, Graduate School of Science and Technology, Shinshu University, 4-17-1 Wakasato, Nagano 380-8553, Japan*

[2]*Research & Development Division, Process Development Department, Shinko Electric Industries Co., Ltd., 36 Kita-Owaribe, Nagano 381-0014, Japan*

* Corresponding author

E-mail: nishiki@shinshu-u.ac.jp

Phone: +81-26-269-5536

FAX: +81-26-269-5550

Abstract

Cu-doped TiO_2 was prepared by the refluxing of a mixture of copper and titanium alkoxides. The refluxing improved the Cu^{2+} dispersion in the TiO_2 and formed effective Ti-O-Cu bonds. The impurity states due to the highly dispersed Cu^{2+} were presumed to trap the electrons in the conduction band of the TiO_2 and prevent charge recombination of the electrons and holes. Consequently, the prolonged charge separation duration was suggested to enhance the photocatalytic activity of the Cu-doped TiO_2. This enhancement was confirmed by the hydroxyl radical generation and organic compound degradation. The Ti-O-Cu bonds and electronic interaction between Cu and Ti should effectively promote the electron trapping. The Cu-doped TiO_2 exhibited a visible light-induced activity due to the transition from the TiO_2 valence band to the Cu^{2+} impurity states.

Keywords: Cu-doped TiO_2; Refluxing; Metal alkoxides; Sol-gel method; Photocatalysis

Introduction

The technology of photocatalysis has been developed in order to create renewable energy and purify pollutants or harmful compounds impacting the earth's environment. Although TiO_2 is one of many excellent photocatalysts, it only functions during the irradiation of UV light shorter than around 400 nm because it has a band-gap energy of about 3.0 eV [1,2]. The visible-light-driven photocatalysts are required in order to utilize solar and household light [2]. In addition, the fast recombination of the electrons and holes produced by the charge separation is one of the serious problems for producing effective photocatalytic reactions. The metal doping of TiO_2 forms impurity states between its conduction and valence bands, just below the edge level of the conduction band. This is effective in not only visible activation due to electron transition from the valence band to the impurity states but also in prolonging the charge separation lifetime due to trapping the electron in the conduction band [3,4]. Therefore, many scientists have investigated the preparation, structure, and activity of metal-doped TiO_2 because its action mechanism is simple and it is readily available [2].

Choi et al. improved the photocatalytic activity of TiO_2 by the systematic investigation of doping with V, Fe, Mo, Ru, Re, and Os [5]. However, aggregation of the dopants during heat treatment at high temperature was an important problem of inactivation. Irie et al. enabled the visible activation of TiO_2 and the effective reduction of oxygen by the electrons

trapped in the Cu impurity states from the conduction band of TiO_2 [6,7]. One of the wet-methods, i.e., the sol-gel method, is used to obtain uniform TiO_2 nano-sized crystalline particles [8,9]. The metal-doped TiO_2 can be prepared from a sol-gel precursor solution containing various metal compounds [3,10−12]. Metal salts are frequently used as a metal source for metal-doping by the sol-gel method, whereas metal alkoxides are more available for the homogeneous mixing with the main alkoxide [13−15]. It is important that the metal species are homogeneously dispersed on the TiO_2 surface in order to provide an effective electronic interaction between the TiO_2 and the metal. One of the transition metals, copper, is a relatively available and effective dopant for trapping the electrons in the conduction band of TiO_2 [3,4].

In this study, we tried to prepare Cu-homogeneously doped TiO_2 by the sol-gel method via refluxing of the alkoxide solution. Copper(II) isopropoxide and copper(II) nitrate were used as the copper source. The characterization of the prepared photocatalyst samples was accomplished by SEM observations and XRD, XPS, volumetric gas adsorption, and UV-vis spectral analyses. The UV and visible photocatalytic activities of this sample were examined by the degradation of methylene blue and trichloroethylene (TCE) and hydroxyl radical production. The influences of the conformation of the Cu-doping of TiO_2 and the electronic interaction between the Ti and Cu on the photocatalytic activity were discussed.

Experimental

Materials

Titanium tetraisopropoxide (TTIP), copper(II) isopropoxide, copper(II) nitrate, ethanol, hydrochloric acid (35%), methylene blue trihydrate (MB), TCE, barium sulfate, and sodium hydroxide of S or reagent grades were obtained from Wako Pure Chemicals and used without further purification. Reagent-grade terephthalic acid was obtained from Tokyo Kasei and used without further purification. The dry nitrogen gas and dry air gas (ca. nitrogen 79% + oxygen 21%) were obtained from Okaya Sanso. The water was deionized and distilled by a distiller (Yamato WG23).

Preparation of photocatalysts

The sol-gel systems used to prepare the Cu-doped TiO_2 consisted of 15.0 cm^3 of TTIP, copper(II) isopropoxide or copper(II) nitrate (0.10, 1.0, and 10 mol% of the Ti amount), 15.0 cm^3 of ethanol, and 0.080 cm^3 of hydrochloric acid (1.0×10^{-2} mol dm^{-3}) as a catalyst for the sol-gel reaction. The two preparation procedures are explained in detail as follows.

First, copper(II) isopropoxide or copper(II) nitrate and ethanol were mixed and agitated. TTIP was dropwise added to the mixtures in a glove box filled with dry nitrogen gas at ambient temperature. The sol-gel reaction started by adding hydrochloric acid. The resulting sols containing copper(II) isopropoxide or copper(II) nitrate were labeled Sol-n-CuA and Sol-n-CuN, respectively. The sol containing TTIP without Cu, Sol-n, was also

prepared. The gelation of these systems occurred 10−14 days after starting the reaction at 60 °C.

Second, TTIP and copper(II) isopropoxide or copper(II) nitrate were mixed and agitated in a glove box filled with dry nitrogen gas at ambient temperature. These mixtures were refluxed at 60 °C for 3 h. Ethanol and hydrochloric acid were added to the refluxed mixtures and their sol-gel reaction started. The resulting sols containing copper(II) isopropoxide or copper(II) nitrate were labeled Sol-r-CuA and Sol-r-CuN, respectively. The sol containing TTIP without Cu, Sol-r, was also prepared. The gelation of these systems occurred 7−10 days after starting the reaction at 60 °C.

All the resulting dry gels were treated with 50 cm^3 of water at 80 °C, heated at 100 °C for 2 h, and then heated at 500 °C for 2 h. The photocatalyst samples were labeled as shown in Table 1.

Characterization of photocatalysts

The prepared photocatalyst samples were characterized by SEM observations using a field emission scanning electron microscope (Hitachi S-4000), XRD analysis by CuKα radiation using an X-ray diffractometer (Rigaku RINT2000), and XPS by AlKα radiation using an X-ray photoelectron spectrophotometer (ULVAC PHI 5600). The size of the crystallites of each sample was estimated from the full-width at half-maximum of the 25.3° peak in the XRD pattern using Sherrer's equation, $D = 0.9\lambda/\beta \cdot \cos\theta$. The specific surface areas,

average pore sizes, and total pore volumes of the samples were estimated by the BET and BJH methods from the adsorption isotherms of nitrogen gas using a volumetric gas adsorption instrument (BEL Japan, BELSORP-mini) [16,17]. The spectroscopic properties of the samples diluted with barium sulfate powder were analyzed by UV-visible diffuse reflectance spectroscopy using a UV-visible near-IR spectrophotometer (Shimadzu UV3150).

Photocatalytic degradation of MB and TCE

Each photocatalyst sample of 5.0 mg was added to 50 cm^3 of an MB aqueous solution (1.0×10^{-5} mol dm^{-3}) and agitated in the dark for 12 h. It was confirmed that the adsorption of MB was equilibrated. The amount of the MB adsorbed on each sample was estimated from the equilibrium concentration in the MB aqueous solution. The degradation reaction of the MB was carried out in a glass beaker by near-UV light irradiation (300−400 nm, peak at 352 nm) from a 4-W black light bulb (Toshiba FL4BLB) and visible light irradiation from a 150-W xenon lamp (Hamamatsu Photonics C2577) using 420-nm-short cutoff and 550-nm-long cutoff filters (420−550 nm pass). The 550-nm-long cutoff filter was used in order to cut light in the main MB absorption band and prevent the MB excitation. The UV-vis absorption spectra of the centrifuged solutions were obtained as a function of the light irradiation time using a UV-visible near-IR spectrophotometer (Shimadzu UV3150). The concentration of MB was estimated from the absorbance at the peak wavelength of 664 nm.

Each 250-mg photocatalyst sample was placed in an infrared cell made of Pyrex glass.

Two plates of KBr single crystals were used as the infrared windows and were sealed by Teflon O-rings. The TCE gas diluted with dry air was injected into the infrared cell in which its concentration was 3.1×10^{-4} mol dm^{-3}. The cell was kept at ambient temperature until the TCE adsorption had equilibrated. The degradation reaction of the TCE was carried out in the cell by the near-UV and visible light irradiations as already stated. The FTIR spectra of the gas phase in the cell were obtained as a function of the light irradiation time using a Fourier transform infrared spectrophotometer (Shimadzu IRPrestige-21). The changes in the concentrations of TCE and the products were determined during the TCE degradation using the prepared photocatalyst samples.

Hydroxyl radical detection

Each 5.0 mg photocatalyst sample was added to 50 cm^3 of terephthalic acid (3.0×10^{-3} mol dm^{-3}) and sodium hydroxide (1.0×10^{-2} mol dm^{-3}). The suspensions were agitated in a glass beaker during the near-UV light and visible light irradiations as already described. The reaction between the terephthalic acid and hydroxyl radical resulting from the photocatalytic water oxidation produces 2-hydroxy terephthalic acid [18,19]. The fluorescence spectra of the 2-hydroxy terephthalic acid in the centrifuged solutions upon 312-nm excitation were obtained as a function of the light irradiation time using a fluorescence spectrophotometer (Shimadzu RF5300).

Results and discussion

Characterization of the photocatalysts

Figure 1 shows the SEM images of the prepared photocatalyst samples, the TiO_2 and Cu-doped TiO_2 prepared from the untreated and refluxed sols containing only TTIP, TTIP and copper(II) isopropoxide, or TTIP and copper(II) nitrate. As shown in Table 2, the average particle sizes of the samples were estimated by measuring their apparent sizes, i.e., diameters of the spherical particles or diagonal lengths of the polyhedron particles, in the images. The particle sizes of the Cu-doped TiO_2 samples are larger than those of the TiO_2 samples. The large aggregates observed in the r-CuN100-TiO_2 sample can be assigned to the CuO particles. There were slight differences between the samples prepared from Sol-n-CuA, Sol-n-CuN, Sol-r-CuA, and Sol-r-CuN.

(Fig. 1 and Table 2)

The XRD patterns of all the samples exhibited diffraction peaks that appeared at 25.3, 37.9, 48.1, 53.8, and 55.0° as shown in Fig. 2. These peaks coincided with the typical pattern for the anatase-type TiO_2. The crystallite sizes were estimated from the strongest peaks at 25.3° as shown in Table 3. In addition, CuO peaks were also observed at 35.4 and 38.6° in the samples containing 10 mol% Cu, especially r-CuN100-TiO_2. The aggregates shown in the SEM image of this sample should be the deposited CuO crystals. These results indicated that Cu was incorporated into the TiO_2 networks and substituted for Ti in the

systems containing an amount of Cu less than 10 mol% Ti. The crystallite sizes increased with an increase in the Cu amount because the substitution of Cu (with the ion radius of 0.072 nm) with Ti (with the ion radius of 0.068 nm) caused lattice strain and promoted the crystal growth [12]. However, the higher amount of Cu cannot be incorporated into the TiO_2 networks and therefore precipitated. The higher deposition of CuO in the Cu-doped TiO_2 samples prepared from the Sol-r-CuN (r-CuN***-TiO_2) is because the affinity of the Cu(II) nitrate with TTIP is lower than that of the Cu(II) isopropoxide.

(Fig. 2 and Table 3)

The crystallite sizes of the Cu-doped TiO_2 samples are different from their particle sizes estimated from the SEM images. The crystallite size depends on the rates of the phase transition of the systems or the nucleation and nuclear growth during heating [20,21]. Refluxing of the sols promoted the polymerization of the metal alkoxides and reorientation due to effectively heating the systems. Consequently, a higher amount of nuclei was produced and individually grew into the relatively smaller crystallites. The specific surface areas of the samples are related to the particle sizes. The larger particle size of the Cu-doped TiO_2 is because the oxygen defects induced the hydrophilic surface of the particles and their agglomeration to form larger secondary particles.

The specific surface areas, average pore sizes, and total pore volumes of the samples are summarized in Table 4.

(Table 4)

Figures 3 and 4 show the XPS spectra relating the binding energy of the Ti 2p and O 1s electrons, respectively, for all the samples. The Ti 2p spectra of the undoped TiO_2 samples, n-TiO_2 and r-TiO_2, exhibited peaks at 464.5 and 458.7 eV assigned to the typical Ti^{4+} [22]. The peaks did not depend on the Cu content in the Cu-doped TiO_2 samples prepared from the Sol-n-CuA and Sol-r-CuN (n-CuA***-TiO_2 and r-CuN***-TiO_2). On the other hand, the peaks were shifted to the higher energy side with an increase in the Cu content of the Cu-doped TiO_2 samples prepared from Sol-n-CuN and Sol-r-CuA (n-CuN***-TiO_2 and r-CuA***-TiO_2). The peak value of the lower energy bands for n-CuN100-TiO_2 and r-CuA100-TiO_2 was 459.8 eV. This is due to the electronic interaction between Ti^{4+} and Cu^{2+}, whose Pauling electronegativities are 1.54 and 1.90, respectively [4,23−25]. As Cu ions are homogeneously dispersed in TiO_2 and substituted for Ti^{4+} in the networks, a charge transfer from the Ti^{4+} to the Cu^{2+} is expected to occur. During the preparation of the sample, n-CuA***-TiO_2, the reactivity between TTIP and Cu(II) isopropoxide were low in the ethanol-based sol due to the difference in their hydrolysis rates, which induced the nucleation and growth of CuO due to easily oxidized Cu. Refluxing of the two metal alkoxides was effective in forming the Ti-O-Cu bonds [26]. During the preparation of the n-CuN***-TiO_2 sample, the Ti-O-Cu bonds were also easily formed based on the Ti 2p peak shift. Cu(II) nitrate was easily dissolved to produce Cu^{2+} in the ethanol-based sol and can easily react with

TTIP during the sol-gel reaction even without refluxing. Refluxing of such sols promoted the growth of CuO due to the faster reaction rate of Cu^{2+} than TTIP.

The O 1s peaks were observed at 530.1 eV in the TiO_2 samples and they were shifted to the higher energy side with an increase in the Cu content. The peak values for all the Cu 10%-doped samples were in the 530.8−531.0 eV range. The shift is because the increase in the amount of oxygen defects, compared to that of the lattice oxygen, caused the formation of hydroxyl oxygen and the adsorption of oxygen [4]. The Cu 2p peaks were observed at 934, 943, 955, and 962 eV in only the samples containing 10 mol% Cu (not shown) due to its detection limit. These peaks were assigned to the Cu^{2+} species [27].

(Fig. 3)

Figure 5 shows the UV-visible diffuse reflectance spectra of the TiO_2 and Cu-doped TiO_2 prepared from Sol-r and Sol-r-CuA, respectively (r-TiO_2 and r-CuA***-TiO_2). The ordinate indicates the Kubelka-Munk function approximating the absorbance. The Cu-doped TiO_2 samples obviously exhibit a visible light absorption ranging from 400 to 550 nm, whereas the absorption edge of the undoped TiO_2 sample is located at around 400 nm. Therefore, the Cu-doped TiO_2 probably more efficiently utilizes visible light than the undoped TiO_2. This result indicated that Cu^{2+} was definitely doped into the TiO_2 and formed impurity states just below the edge level of the conduction band of the TiO_2 because the shifts in the absorption edge for the samples correspond to the amount of the doped Cu^{2+} [6,7,12].

(Fig. 5)

Photocatalytic degradation of MB during UV irradiation

Figure 6 shows the specific surface area of the photocatalyst samples, the TiO_2 and Cu-doped TiO_2 prepared from the sol containing Sol-r and Sol-r-CuA, respectively (r-TiO_2 and r-CuA***-TiO_2), and the amount of the MB adsorbed on them. The specific surface area decreased with an increase in the Cu content due to the crystal growth and decrease in the mesopore volume. The MB adsorption amounts of the samples did not correlate with their specific surface areas. Although the specific surface area of r-TiO_2 was higher than those of r-CuA001-TiO_2 and r-CuA010-TiO_2, the MB absorption amount of r-TiO_2 was less than that of r-CuA001-TiO_2 and not remarkably different from that of r-CuA010-TiO_2. The MB adsorption ability is suggested to increase with an increase in the surface hydrophilicity because the amount of the hydroxyl groups on the TiO_2 surface increased with an increase in the Cu content based on the XPS analysis [28]. Both the specific surface area and MB adsorption amount of r-CuN100-TiO_2 were the lowest of all the samples due to significant progress in the crystal growth of TiO_2 and CuO.

(Fig. 6)

Figures 7 and 8 show the changes in the UV-vis absorption spectra of MB in the aqueous solutions and the time course of its concentration, respectively, during the UV photocatalytic degradation using the TiO_2 and Cu-doped TiO_2 prepared from Sol-r and Sol-r-CuA,

respectively (r-TiO_2 and r-CuA***-TiO_2). The irradiation to produce the photocatalytic reaction was conducted after the adsorption of MB had equilibrated. The MB absorption peaks at 664 nm were blue-shifted with the irradiation time, indicating the dissociation of the *N,N*-dimethyl amino groups of MB due to the oxidative degradation by the holes charge-separated in the photocatalysts [29−33]. The decreases in the absorbance by the UV irradiation are mainly due to the ring-opening reaction of MB by the holes or the hydroxyl radicals produced from the water oxidation. The MB concentrations fast and significantly decreased using the photocatalyst samples compared to that without any photocatalysts. MB was slightly degraded by only UV light because it exhibits a UV absorption. The present photocatalyst samples remarkably promoted the MB degradation. The photocatalysts prepared in this study exhibited almost the same light absorption properties in the UV region due to the small amount of Cu doping and their MB adsorption amounts were not significantly different compared to those of the photocatalytically degraded MB. Therefore, the degradation rate of MB using each photocatalyst sample indicates its photocatalytic activity related to the reaction quantum yield. The r-CuA001-TiO_2 sample exhibited the highest photocatalytic activity based on the MB degradation rate. This is because r-CuA001-TiO_2 has the highest MB adsorption ability and relatively high specific surface area. The higher amount of Cu decreased the photocatalytic activity due to the decreases in the specific surface area, hydrophilicity, and light permeation. The Ti-O-Cu

bond formation by the Cu-doping is expected to effect prolongment of the charge separation duration.

(Figs. 7 and 8)

Figure 9 shows the specific surface areas of the photocatalyst samples, n-TiO_2, n-CuA001-TiO_2, n-CuN001-TiO_2, r-TiO_2, r-CuA001-TiO_2, and r-CuN001-TiO_2, and the amounts of the MB adsorbed on them. The MB adsorption ability depended on the specific surface area and the surface hydrophilicity. The Cu-doped TiO_2 samples, except for r-CuN001-TiO_2, exhibited a relatively high MB adsorption because their particle surfaces were more hydrophilic than those of the TiO_2 samples based on the results of the XPS analysis. On the other hand, r-CuN001-TiO_2 is suggested to have a less hydrophilic surface because the amounts of the Ti-O-Cu bond and oxygen defects were lower than those of r-CuA001-TiO_2 and n-CuN001-TiO_2.

(Fig. 9)

Figure 10 shows the time course of the MB concentration in the aqueous solutions during the UV photocatalytic degradation using n-TiO_2, n-CuA001-TiO_2, n-CuN001-TiO_2, r-TiO_2, r-CuA001-TiO_2, and r-CuN001-TiO_2. The MB degradation performances of n-CuA001-TiO_2 and n-CuN001-TiO_2 were higher than that of n-TiO_2 due to the Cu-doping effect. The samples, r-TiO_2 and r-CuA001-TiO_2, exhibited higher activities for the MB degradation than n-TiO_2 and n-CuA001-TiO_2, respectively, indicating the effectiveness of

refluxing to produce fine crystals and their high surface area and adsorption ability. However, the activity of r-CuN001-TiO_2 decreased by refluxing due to the CuO aggregation. Consequently, r-CuA001-TiO_2 exhibited the highest photocatalytic performance. We strongly suggested that the formation of the Ti-O-Cu bonds can effectively increase the photocatalytic activity.

(Fig. 10)

Figures 11 and 12 show the time course of the fluorescence intensity of 2-hydroxy terephthalic acid in order to detect the hydroxyl radical produced during the UV irradiation and photocatalytic water splitting. The intensity values at 426 nm in the fluorescence spectra upon 312-nm excitation were plotted versus the irradiation time. The amount of the produced hydroxyl radical depended on the photocatalytic activity of the individual samples, which correlated to their MB degradation performances. This result indicated that the MB molecules were degraded by the hydroxyl radicals in the aqueous solutions. In addition, the holes probably degraded the MB adsorbed on the photocatalyst surface.

(Figs. 11 and 12)

Photocatalytic degradation of MB during visible irradiation

Figure 13 shows the time course of the concentration of MB in the aqueous solutions during the visible photocatalytic degradation using r-TiO_2 and r-CuA001-TiO_2. The photocatalytic degradation was conducted after the adsorption of MB had equilibrated. As

expected, MB was slightly degraded using r-TiO_2 due to no absorption of visible region similar to the result without any photocatalyst. MB was very slowly degraded using r-CuA001-TiO_2 during the visible irradiation compared to the result during the UV irradiation. The MB degradation performances of r-CuA001-TiO_2 were due to the visible light absorption effect of the Cu-doping.

(Fig. 13)

Figure 14 shows the time course of the fluorescence intensity of 2-hydroxy terephthalic acid in order to detect the hydroxyl radical produced during the visible irradiation under the above conditions. The undoped r-TiO_2 slightly produced hydroxyl radicals as expected from the above MB degradation result. A certain amount of the hydroxyl radical was produced using r-CuA001-TiO_2 even though it required a much longer time than during the UV irradiation. This result indicated that the photocatalytic activity resulted from the electron excitation and charge separation due to the transition from the TiO_2 valence band to the Cu^{2+} impurity states. The charge separation lifetime in the photocatalyst was enough to produce the required amount of hydroxyl radicals for the MB degradation.

(Fig. 14)

Photocatalytic degradation of TCE during UV and visible irradiations

The photocatalytic degradation reactions of TCE were investigated using the prepared samples, r-TiO_2 and r-CuA001-TiO_2, upon UV or visible irradiation. The three typical

characteristic IR bands of TCE at 944 cm^{-1} (C-Cl stretching), 849 cm^{-1} (C-Cl stretching), and 783 cm^{-1} (C-H bending) rapidly decreased during the UV irradiation. In addition to these changes, CO (2231–2066 cm^{-1}), CO_2 (2398–2280 cm^{-1}), $COCl_2$ (856 cm^{-1}), HCl (3037–2723 cm^{-1}), and DCAC (800 and 741 cm^{-1}) were mainly produced during the reaction [34−39]. The degradation of TCE was confirmed by these IR measurements as reported in the literature [34,36,37,40−44]. During the visible irradiation, TCE was degraded and CO, CO_2, HCl, and $COCl_2$ were generated as well as during the UV irradiation. However, no DCAC was found in this case similar to the results reported in a previous paper [34,44].

The amounts of TCE and each product were estimated by analyzing their FTIR spectra. Figure 15 shows the time course of the TCE concentration estimated from the IR absorbance at 944 cm^{-1} during UV and visible irradiations. TCE was degraded during the 7–10 min UV irradiation using the prepared samples, indicating that the two samples functioned as highly active photocatalysts. The degradation rate of TCE during the UV irradiation using r-Cu-A001-TiO_2 was faster than using r-TiO_2. The activity of the photocatalyst samples strongly depended on their specific surface area and electron trapping effect rather than their crystallinity because their crystallite sizes were not very different. The contribution of the hydroxyl radicals to the TCE degradation should be low in the present systems because a slight amount of water molecules was present in the gas phase. Therefore, the reaction of TCE with the adsorbed oxygen molecules on the catalyst surface is an important process

during the TCE degradation, which is certainly induced by the oxygen adsorption and the charge separation to form Ti^{3+} species [8,36,44−46].

(Fig. 15)

TCE was definitely degraded during the visible irradiation using r-CuA001-TiO_2 whereas its concentration slightly decreased using r-TiO_2. This indicates the visible light-induced activity of the r-CuA001-TiO_2. However, it took much a longer time to degrade the TCE during the visible irradiation than during the UV irradiation due to low absorbance in the visible region. The visible light-induced activity of the Cu-doped TiO_2 is due to the transition from the TiO_2 valence band to the Cu^{2+} impurity states.

Conclusions

TiO_2 was homogeneously doped with Cu using the sol-gel method by refluxing of a mixture of copper and titanium alkoxides compared to the mixture of a copper salt and titanium alkoxide. This was confirmed by SEM observations and XRD, XPS, volumetric gas adsorption, and UV-vis spectral analyses. The refluxing of the mixture of copper and titanium alkoxides improved the Cu^{2+} dispersion in the TiO_2 and formed effective Ti-O-Cu bonds, whereas that of the mixture of a copper salt and a titanium alkoxide caused CuO aggregation. The UV and visible photocatalytic activities of this sample were examined by the degradations of MB and TCE and the hydroxyl radical production. The impurity states

due to the highly dispersed Cu^{2+} was presumed to trap the electron in the conduction band of the TiO_2 and prevent the charge recombination of the electrons and holes. Consequently, the prolonging of the charge separation duration was suggested to enhance the photocatalytic activity of the Cu-doped TiO_2. The Ti-O-Cu bonds and electronic interaction between the Cu and Ti should effectively promote the electron trapping. The Cu-doped TiO_2 exhibited a visible light-induced activity due to the transition from the TiO_2 valence band to the Cu^{2+} impurity states.

Acknowledgments

The authors thank Prof. Kenichi Tenya of this university for his technical assistance with the XPS analysis. The authors also thank Prof. Tomohiko Okada of this university for his technical assistance with the volumetric gas adsorption analysis.

References

[1] A. Fujishima, T. N. Rao, D A. Tryk, J. Photochem. Photobiol. C-Photochem. Rev. 1, 1 (2000)

[2] D. Chatterjee, S. Dasgupta, J. Photochem. Photobiol. C-Photochem. Rev. 6, 186, (2005)

[3] G. Colón, M. Maicu, M. C. Hidalgo, J. A. Navío, Appl. Catal. B-Environ. 67, 41

(2006)

[4] B. Xin, P. Wang, D. Ding, J. Liu, Z. Ren, H. Fu, Appl. Surf. Sci. 254, 2569 (2008)

[5] W. Choi, A. Termin, M. R. Hoffmann, J. Phys. Chem. 98, 1369 (1994)

[6] H. Irie, S. Miura, K. Kamiya, K. Hashimoto, Chem. Phys. Lett. 457, 202 (2008)

[7] H. Irie, K. Kamiya, T. Shibanuma, S. Miura, D. A. Tryk, T. Yokoyama, K. Hashimoto, J. Phys. Chem. C 113, 10761 (2009)

[8] H. Nishikiori, M. Tagahara, L. Mukoyama, T. Fujii, Res. Chem. Intermed. 36, 947 (2010)

[9] H. Nishikiori, M. Furukawa, T. Fujii, Appl. Catal. B-Environ. 102, 470 (2011)

[10] E. Celik, Z. Gokcen, N. F. Ak Azem, M. Tanoglu, O. F. Emrullahoglu, Mater. Sci. Eng. B 132, 258 (2006)

[11] I. H. Tseng, J. C. S. Wu, H. Y. Chou, J. Catal. 221, 432 (2004)

[12] R. López, R. Gómez, M. E. Llanos, Catal. Today 148, 103 (2009)

[13] R. C. Mehrotra, J. Non-Cryst. Solids 100, 1 (1988)

[14] T. Monde, H. Kozuka, S. Sakka, Chem. Lett. 17, 287 (1988)

[15] T. Satoh, M. Ogawa, M. Kondo, J. Ceram. Soc. Jpn. 106, 1151 (1998)

[16] S. Brunauer, P. H. Emmett, E. Teller, J. Am. Chem. Soc. 60, 309 (1938)

[17] E. P. Barrett, L. G. Joyner, P. H. Halenda, J. Am. Chem. Soc. 73, 373 (1951)

[18] T. Hirakawa, Y. Nosaka, Langmuir 18, 3247 (2002)

[19] T. Hirakawa, K.Yawata, Y. Nosaka, Appl. Catal. A-Gen. 325, 105 (2007)

[20] H. Yin, Y. Wada, T. Kitamura, S. Kambe, S. Murasawa, H. Mori, T. Sakata, S. Yanagida, J. Mater. Chem. 11, 1694 (2001)

[21] A. J. Maira, K. L. Yeung, C. Y. Lee, P. L. Yue, C. K. Chan, J. Catal. 192, 185 (2000)

[22] J. Yu, X. Zhao, Q Zhao, Mater. Chem. Phys. 69, 25 (2001)

[23] G. Li, N. M. Dimitrijevic, L. Chen, T. Rajh, K. A. Gray, J. Phys. Chem. C 112, 19040 (2008)

[24] Q. Fang, M. Meier, J. J. Yu, Z. M. Wang, J. Y. Zhang, J. X. Wu, A. Kenyon, P. Hoffmann, I. W. Boyd, Mater. Sci. Eng. B 105, 209 (2003)

[25] M. You, T. G. Kim, Y. M. Sung, Cryst. Growth Des. 10, 983 (2010)

[26] L. Pan, J. J. Zou, X. Zhang, L. Wang, Ind. Eng. Chem. Res. 49, 8526 (2010)

[27] W. Zhang, Y. Li, S. Zhu, F. Wang, Catal. Today 589, 93 (2004)

[28] T. Sreethawong, S. Yoshikawa, Catal. Commun. 6, 661 (2005)

[29] T. Zhang, T. Oyama, A. Aoshima, H. Hidaka, J. Zhao, N Serpone, J. Photochem. Photobio. A Chem. 140 (2001) 163

[30] S. Senthilkumaar, K. Porkodi, R. Gomathi, A. G. Maheswari, N. Manonmani, Dyes Pigments 69, 22 (2006)

[31] Z. Yu, S. S. C. Chuang, Appl. Catal. B-Environ. 83, 277 (2008)

[32] H. W. P. Carvalho, A. P. L. Batista, P. Hammer, T. C. Ramalho, J. Hazard. Mater. 184,

273 (2010)

[33] L. Yu, S. Yuan, L. Shi, Y. Zhao, J. Fang, Microporous Mesoporous Mater. 134, 108 (2010)

[34] S. K. Joung, T. Amemiya, M. Murabayashi, K. Itoh, Chem. Eur. J. 12, 5526 (2006)

[35] R. Nakamura, T. Tanaka, Y. Nakato, J. Phys. Chem. B 108, 10617 (2004)

[36] K. Oki, S. Tsuchida, H. Nishikiori, N. Tanaka, T. Fujii, Int. J. Photoenergy 5, 11 (2003)

[37] P. B. Amama, K. Itoh, M. Murabayashi, J. Mol. Catal. A-Chem. 176, 165 (2001)

[38] J. S. Kim, K. Itoh, M. Murabayashi, B. A. Kim, Chemosphere 38, 2969 (1999)

[39] M. Kang, J. H. Lee, S. H. Lee, C. H.Chung, K. J. Yoon, K. Ogino, S. Miyata, S. J. Choung, J. Mol. Catal. A-Chem. 193, 273 (2003)

[40] W. A. Jacoby, M. R. Nimlos, D. M. Blake, R. D. Noble, C. A. Koval, Environ Sci. Technol. 28, 1661 (1994)

[41] J. Fan, J. T. Yates, Jr., J. Am. Chem. Soc. 118, 4686 (1996)

[42] M. D. Driessen, A. L. Goodman, T. M. Miller, G. A. Zaharias, V. V. Grassian, J. Phys. Chem. B 102, 549 (1998)

[43] J. S. Kim, K. Itoh, M. Murabayashi, Chemosphere 36, 483 (1998)

[44] Y. Yokosuka, K. Oki, H. Nishikiori, Y. Tatsumi, N. Tanaka, T. Fujii, Res. Chem. Intermed. 35, 43 (2009)

[45] M. Anpo, Y. Kubokawa, T. Fujii, S. Suzuki, J. Phys. Chem. 88, 2527 (1984)

[46] M. Anpo, T. Shima, T. Fujii, S. Suzuki, Chem. Lett. 16, 1997 (1987)

Table 1 Labels of the prepared photocatalyst samples

	TiO_2	CuA***-TiO_2			CuN***-TiO_2		
		Cu mol%			Cu mol%		
		0.1	1.0	10	0.1	1.0	10
Untreated	n-TiO_2	n-CuA001 -TiO_2	n-CuA010 -TiO_2	n-CuA100 -TiO_2	n-CuN001 -TiO_2	n-CuN010 -TiO_2	n-CuN100 -TiO_2
Refluxed	r-TiO_2	r-CuA001 -TiO_2	r-CuA010 -TiO_2	r-CuA100 -TiO_2	r-CuN001 -TiO_2	r-CuN010 -TiO_2	r-CuN100 -TiO_2

Table 2 Average particle sizes of the prepared catalysts estimated by SEM images

	TiO_2	CuA100-TiO_2	CuN100-TiO_2
Untreated	18	36	28
Refluxed	16	30	36

Table 3 Crystallite sizes of the prepared catalysts estimated by XRD analysis

	TiO_2	CuA***-TiO_2			CuN***-TiO_2		
		Cu mol%			Cu mol%		
		0.1	1.0	10	0.1	1.0	10
Untreated	16	16	17	22	14	16	18
Refluxed	14	13	14	22	11	15	20

Table 4 Pore characteristics of the prepared catalysts estimated by BET and BJH methods from the adsorption isotherms of nitrogen gas measured by the volumetric gas adsorption method

	n-TiO_2	n-CuA001-TiO_2	n-CuN001-TiO_2
Specific surface area / m^2g^{-1}	84	83	71
Average pore size / nm	6.8	6.1	6.6
Total pore volume / cm^3g^{-1}	0.14	0.13	0.12
	r-TiO_2	r-CuA001-TiO_2	r-CuN001-TiO_2
Specific surface area / m^2g^{-1}	111	94	70
Average pore size / nm	6.7	6.1	4.7
Total pore volume / cm^3g^{-1}	0.14	0.14	0.08

Figure captions

Figure 1 SEM images of (a) n-TiO_2, (b) n-CuA100-TiO_2, and (c) n-CuN100-TiO_2 prepared without refluxing, and (d) r-TiO_2, (e) r-CuA100-TiO_2, and (f) r-CuN100-TiO_2 prepared with refluxing

Figure 2 XRD patterns of (a) (1) n-TiO_2, (2) n-CuA001-TiO_2, (3) n-CuA010-TiO_2, and (4) n-CuA100-TiO_2, (b) (1) n-TiO_2, (2) n-CuN001-TiO_2, (3) n-CuN010-TiO_2, and (4) n-CuN100-TiO_2, (c) (1) r-TiO_2, (2) r-CuA001-TiO_2, (3) r-CuA010-TiO_2, and (4) r-CuA100-TiO_2, (d) (1) r-TiO_2, (2) r-CuN001-TiO_2, (3) r-CuN010-TiO_2, and (4) r-CuN100-TiO_2, ○: anatase TiO_2, ●: CuO

Figure 3 XPS spectra of Ti 3d for (a) (1) n-TiO_2, (2) n-CuA001-TiO_2, (3) n-CuA010-TiO_2, and (4) n-CuA100-TiO_2, (b) (1) n-TiO_2, (2) n-CuN001-TiO_2, (3) n-CuN010-TiO_2, and (4) n-CuN100-TiO_2, (c) (1) r-TiO_2, (2) r-CuA001-TiO_2, (3) r-CuA010-TiO_2, and (4) r-CuA100-TiO_2, (d) (1) r-TiO_2, (2) r-CuN001-TiO_2, (3) r-CuN010-TiO_2, and (4) r-CuN100-TiO_2

Figure 4 XPS spectra of O 1s for (a) (1) n-TiO_2, (2) n-CuA001-TiO_2, (3) n-CuA010-TiO_2, and (4) n-CuA100-TiO_2, (b) (1) n-TiO_2, (2) n-CuN001-TiO_2, (3) n-CuN010-TiO_2, and (4) n-CuN100-TiO_2, (c) (1) r-TiO_2, (2) r-CuA001-TiO_2, (3) r-CuA010-TiO_2, and (4) r-CuA100-TiO_2, (d) (1) r-TiO_2, (2) r-CuN001-TiO_2, (3) r-CuN010-TiO_2, and (4) r-CuN100-TiO_2

Figure 5 Diffuse reflectance spectra of (1) r-TiO_2, (2) r-CuA001-TiO_2, (3) r-CuA010-TiO_2, and (4) r-CuA100-TiO_2

Figure 6 Specific surface area and methylene blue adsorption amount of r-TiO_2 (Cu 0%), r-CuA001-TiO_2 (Cu 0.1%), r-CuA010-TiO_2 (Cu 1.0%), and r-CuA100-TiO_2 (Cu 10%)

Figure 7 Changes in UV-vis absorption spectra of methylene blue during its photocatalytic degradation using (a) r-TiO_2, (b) r-CuA001-TiO_2, (c) r-CuA010-TiO_2, and (d) r-CuA100-TiO_2

Figure 8 Time course of concentration of methylene blue during (1) UV irradiation and its photocatalytic degradation using (2) r-TiO_2, (3) r-CuA001-TiO_2, (4) r-CuA010-TiO_2, and (5) r-CuA100-TiO_2 prepared from Sol-r containing Cu isopropoxide

Figure 9 Specific surface area and methylene blue adsorption amount of n-TiO_2, n-CuA001-TiO_2, and n-CuN001-TiO_2, r-TiO_2, r-CuA001-TiO_2, and r-CuN001-TiO_2

Figure 10 Time course of concentration of methylene blue during (1) UV irradiation and its photocatalytic degradation using (2) n-TiO_2, (3) r-TiO_2, (4) n-CuA001-TiO_2, (5) r-CuA001-TiO_2, (6) n-CuN001-TiO_2, and (7) r-CuN001-TiO_2

Figure 11 Time course of fluorescence intensity of 2-hydroxy terephthalic acid in order to detect hydroxyl radical produced during (1) UV irradiation and photocatalytic water splitting using (2) r-TiO_2, (3) r-CuA001-TiO_2, (4) r-CuA010-TiO_2, and (4) r-CuA100-TiO_2

Figure 12 Time course of fluorescence intensity of 2-hydroxy terephthalic acid in order to detect hydroxyl radical produced during (1) UV irradiation and photocatalytic water splitting using (2) n-TiO_2, (3) r-TiO_2, (4) n-CuA001-TiO_2, (5) r-CuA001-TiO_2, (6) n-CuN001-TiO_2, and (7) r-CuN001-TiO_2

Figure 13 Time course of concentration of methylene blue during (1) visible irradiation and photocatalytic water splitting using (2) r-TiO_2, and (3) r-CuA001-TiO_2

Figure 14 Time course of fluorescence intensity of 2-hydroxy terephthalic acid in order to detect hydroxyl radical produced during (1) visible irradiation and photocatalytic water splitting using (2) r-TiO_2, and (3) r-CuA001-TiO_2

Figure 15 Time course of concentration of TCE during its photocatalytic degradation using (1) r-TiO_2 and (2) r-CuA001-TiO_2 during (a) UV and (b) visible irradiations

Figure 1

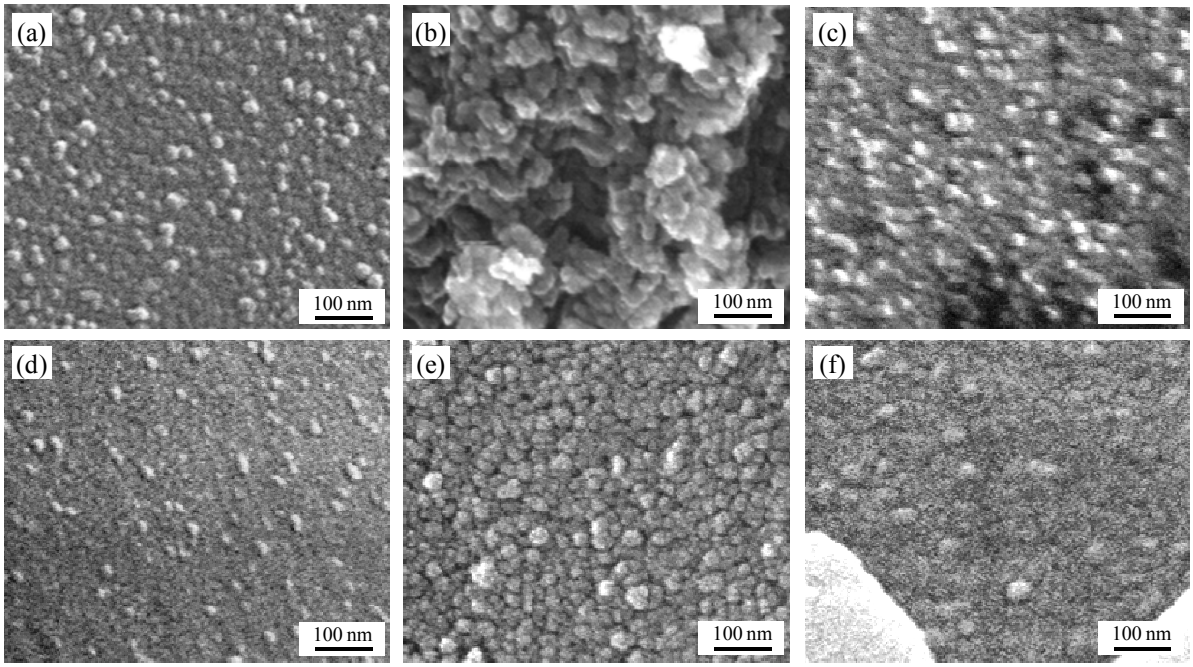

Figure 2

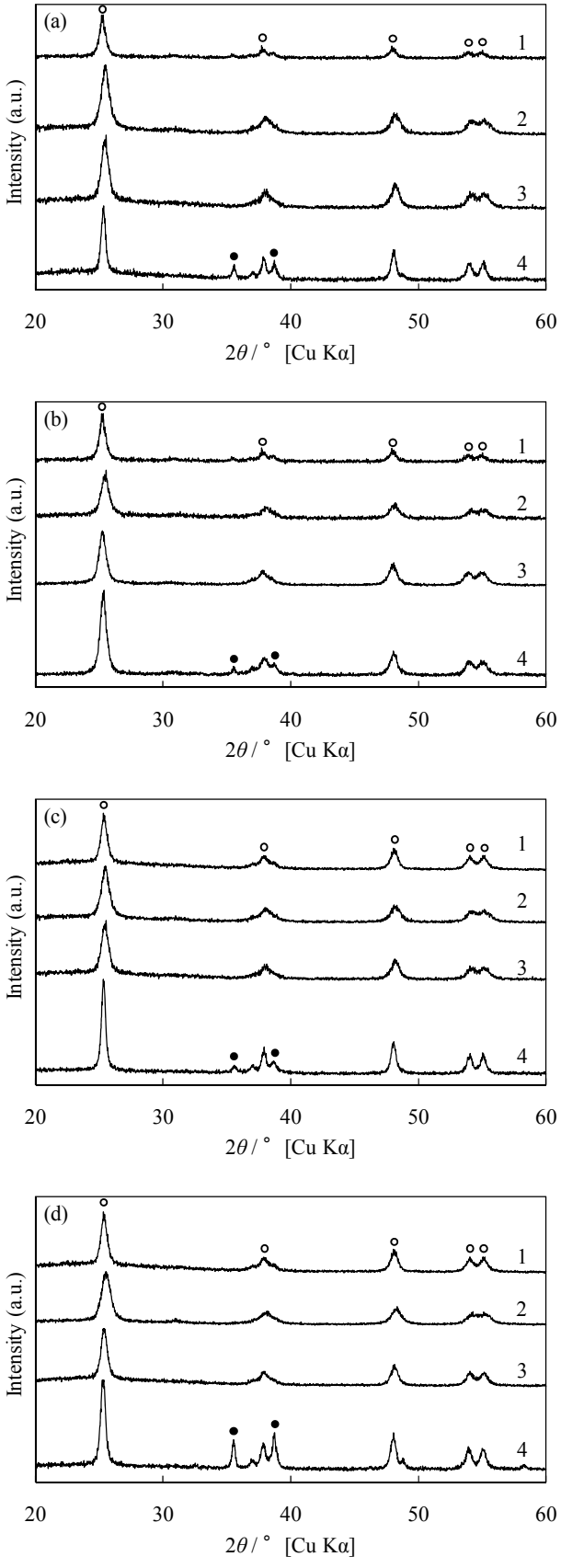

Figure 3

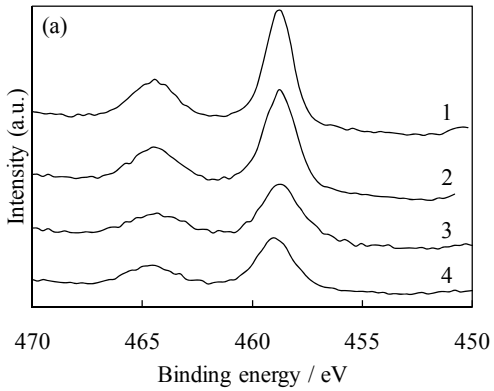
(a)
Intensity (a.u.)
1
2
3
4
470
465
460
455
450
Binding energy / eV

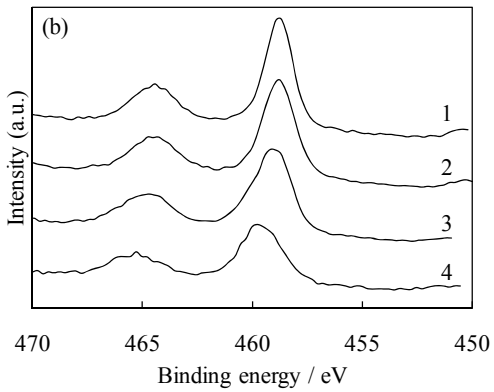
(b)
Intensity (a.u.)
1
2
3
4
470
465
460
455
450
Binding energy / eV

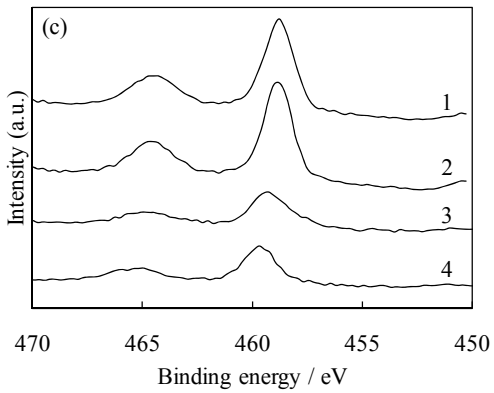
(c)
Intensity (a.u.)
1
2
3
4
470
465
460
455
450
Binding energy / eV

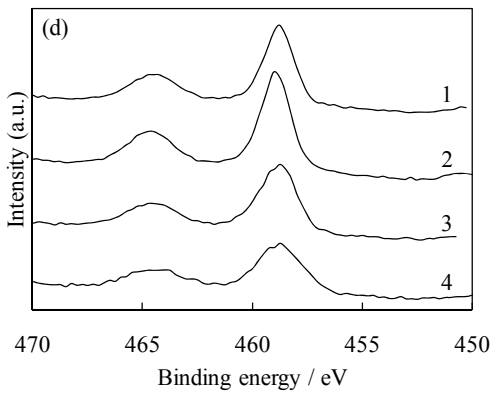
(d)
Intensity (a.u.)
1
2
3
4
470
465
460
455
450
Binding energy / eV

Figure 4

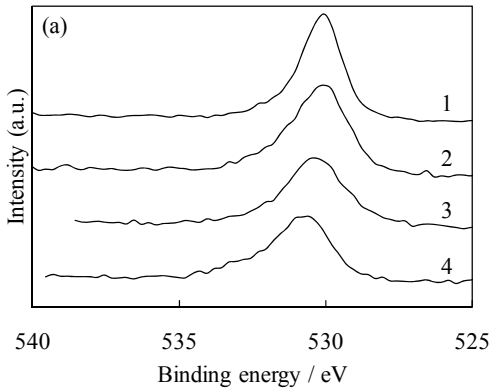
(a)
Intensity (a.u.)
1
2
3
4
540
535
530
525
Binding energy / eV

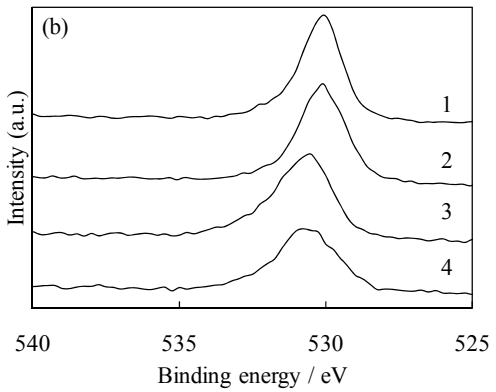
(b)
Intensity (a.u.)
1
2
3
4
540
535
530
525
Binding energy / eV

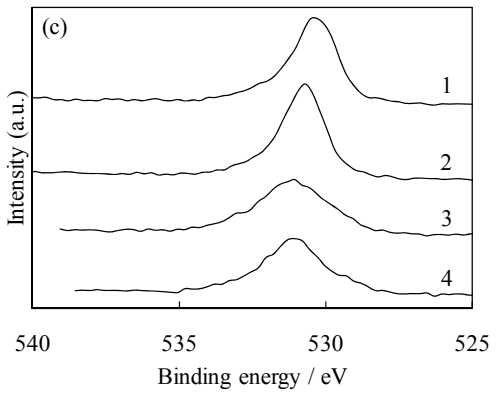
(c)
Intensity (a.u.)
1
2
3
4
540
535
530
525
Binding energy / eV

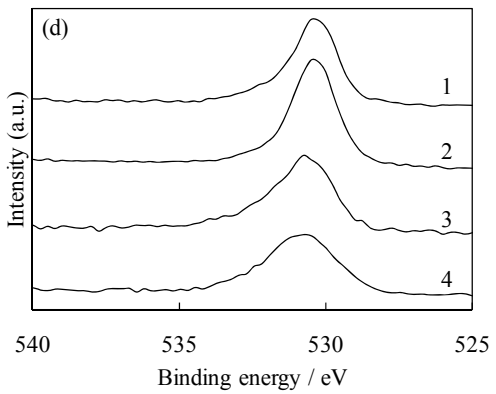
(d)
Intensity (a.u.)
1
2
3
4
540
535
530
525
Binding energy / eV

Figure 5

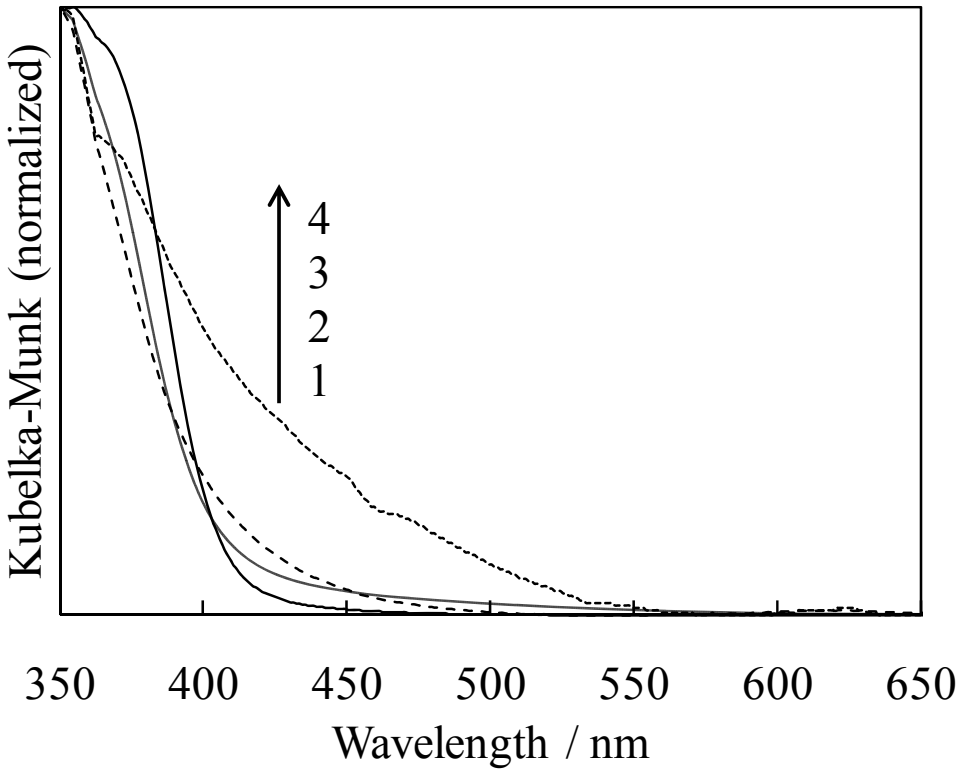
Kubelka-Munk (normalized)
4
3
2
1
350
400
450
500
550
600
650
Wavelength / nm

Figure 6

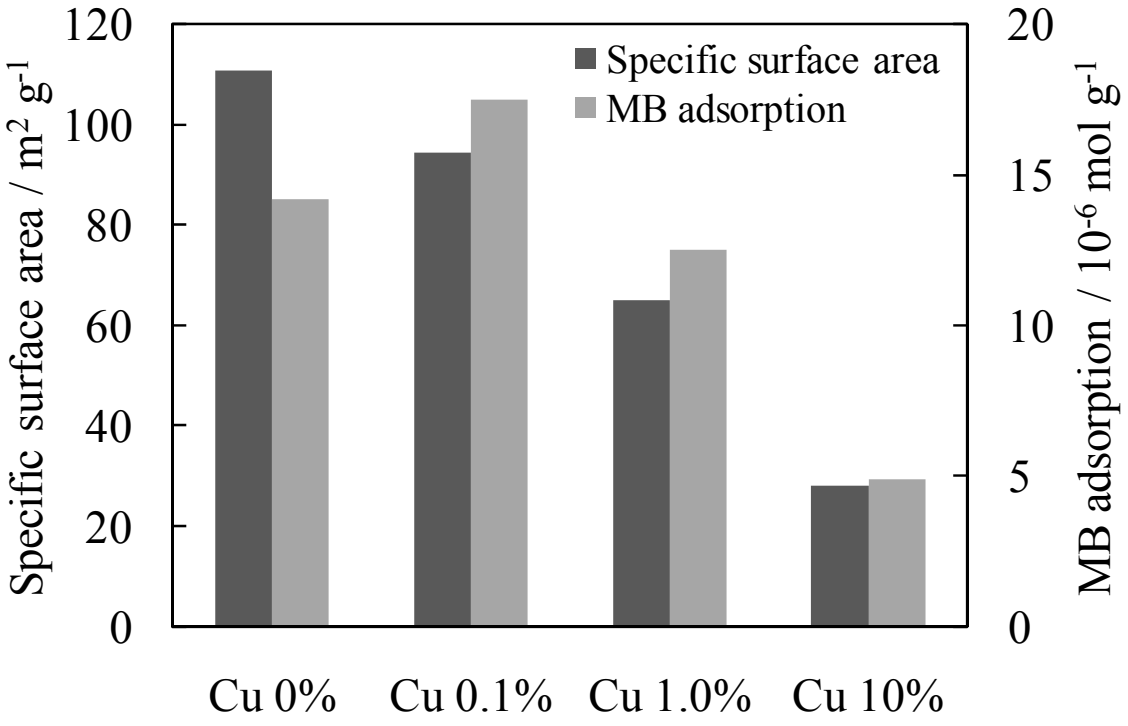
Specific surface area
MB adsorption
Specific surface area / m2 g-1
MB adsorption / 10-6 mol g-1
120
100
80
60
40
20
0
20
15
10
5
0
Cu 0%
Cu 0.1%
Cu 1.0%
Cu 10%

Figure 7

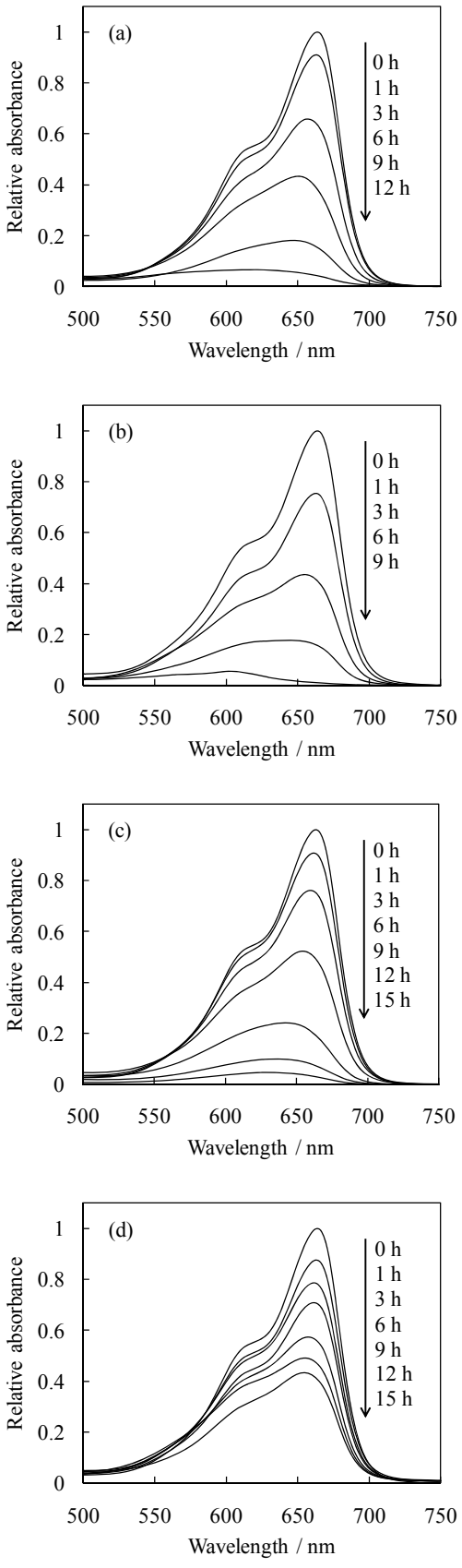
(a)
0 h
1 h
3 h
6 h
9 h
12 h
(b)
0 h
1 h
3 h
6 h
9 h
(c)
0 h
1 h
3 h
6 h
9 h
12 h
15 h
(d)
0 h
1 h
3 h
6 h
9 h
12 h
15 h
Relative absorbance
Wavelength / nm
0
0.2
0.4
0.6
0.8
1
500
550
600
650
700
750

Figure 8

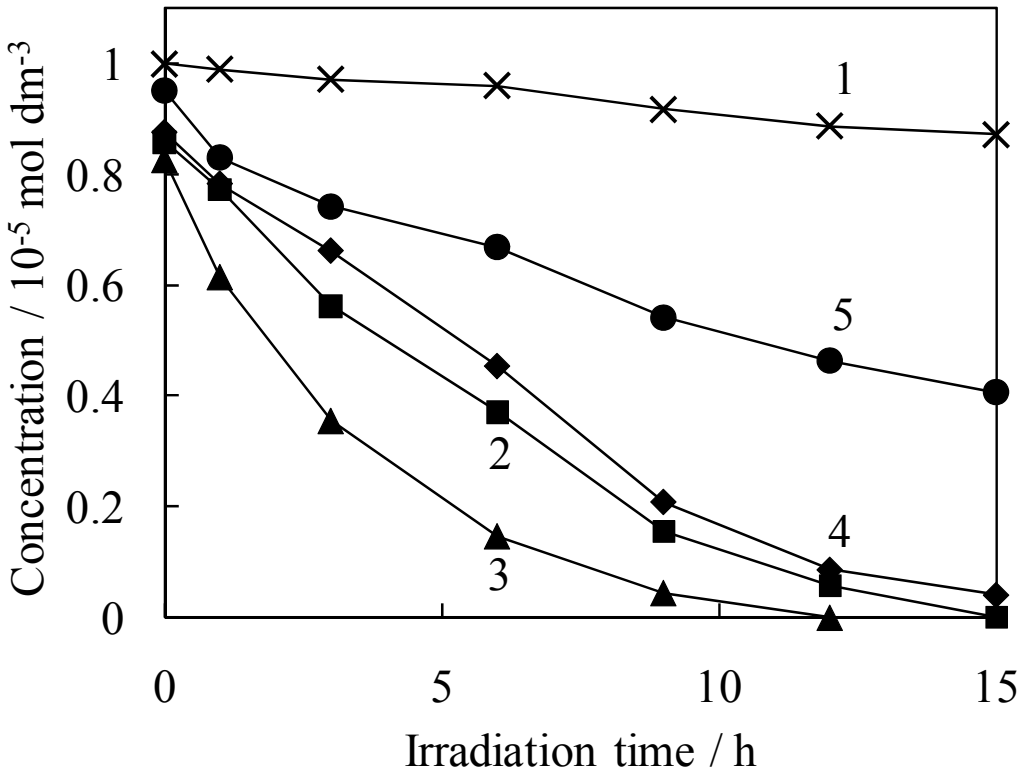
Concentration / 10-5 mol dm-3
1
0.8
0.6
0.4
0.2
0
0
5
10
15
Irradiation time / h
1
5
2
4
3

Figure 9

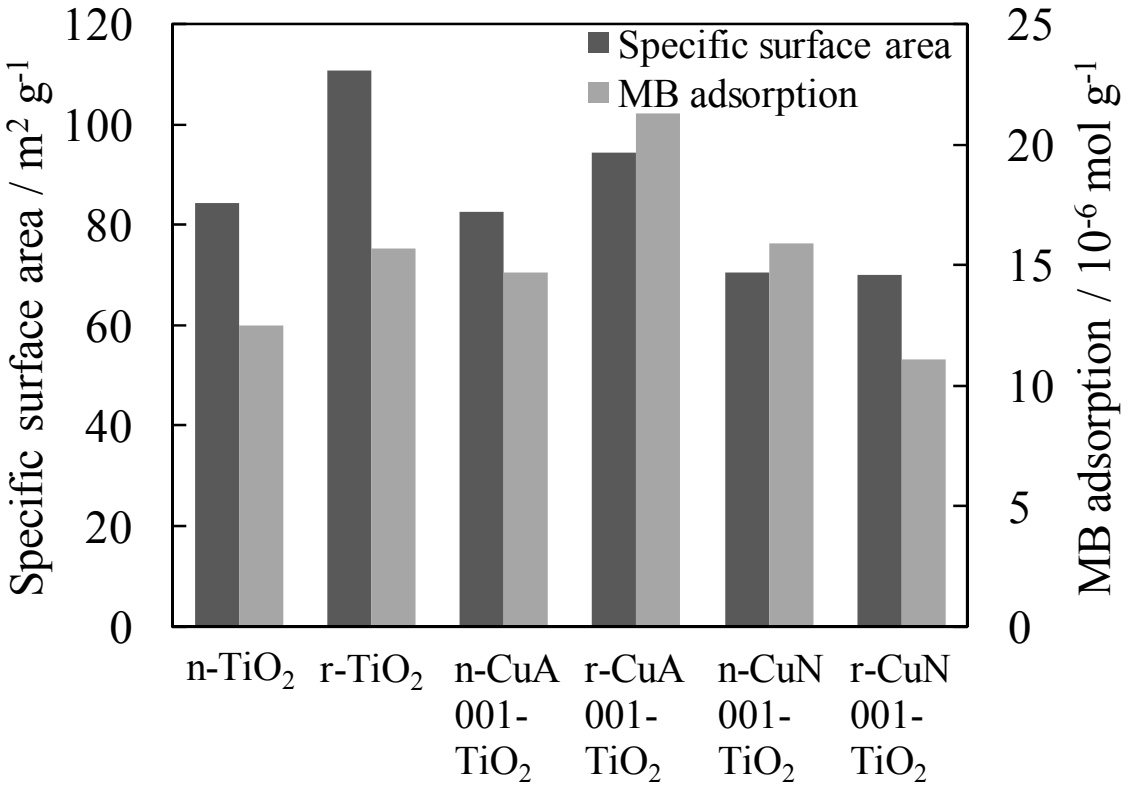
Specific surface area
MB adsorption
Specific surface area / m2 g-1
MB adsorption / 10-6 mol g-1
120
100
80
60
40
20
0
25
20
15
10
5
0
n-TiO2
r-TiO2
n-CuA 001-TiO2
r-CuA 001-TiO2
n-CuN 001-TiO2
r-CuN 001-TiO2

Figure 10

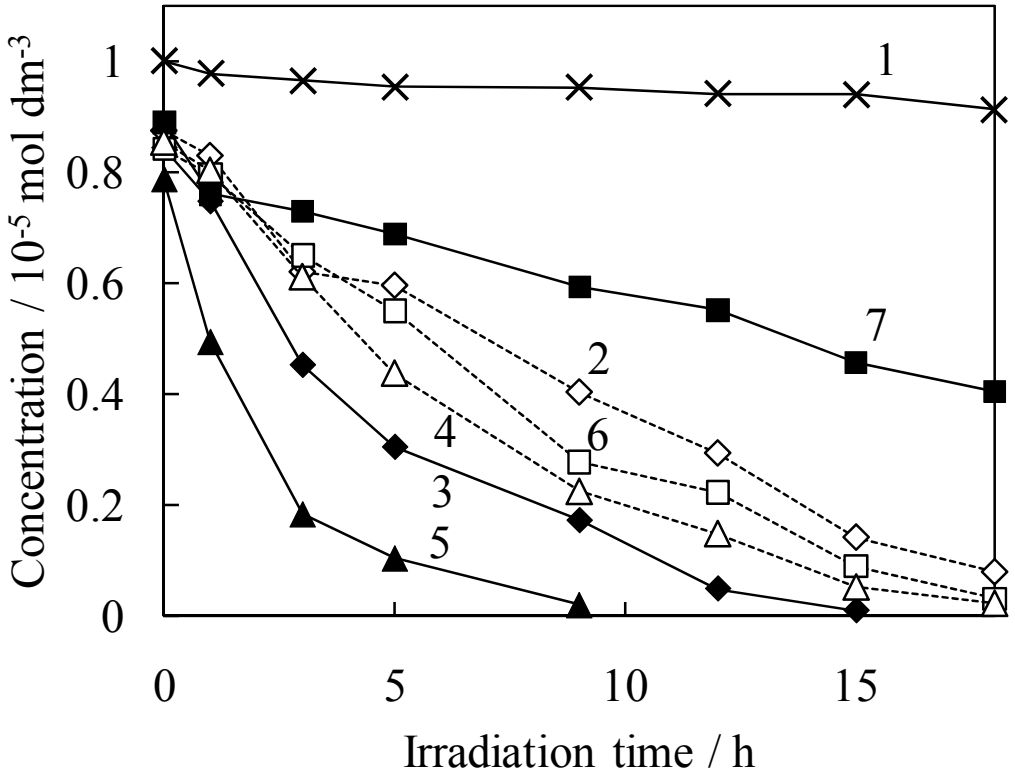
Concentration / 10-5 mol dm-3
1
0.8
0.6
0.4
0.2
0
0
5
10
15
Irradiation time / h
1
7
2
6
4
3
5

Figure 11

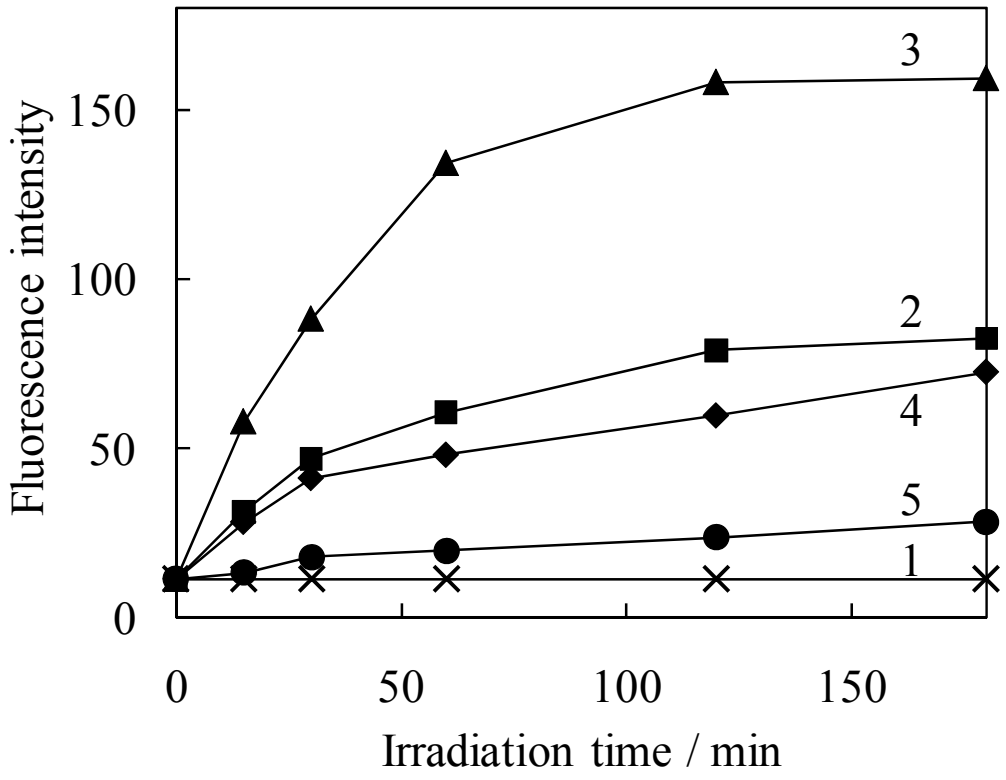
Fluorescence intensity
150
100
50
0
0
50
100
150
Irradiation time / min
3
2
4
5
1

Figure 12

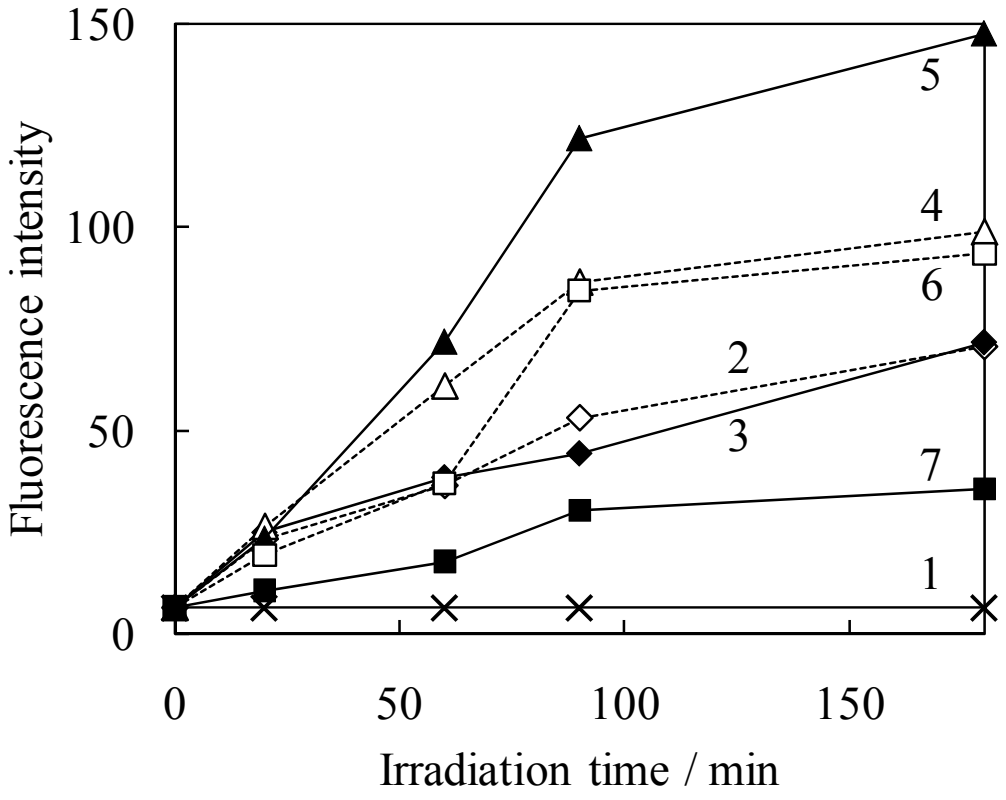
150
100
50
0
Fluorescence intensity
0
50
100
150
Irradiation time / min
5
4
6
2
3
7
1

Figure 13

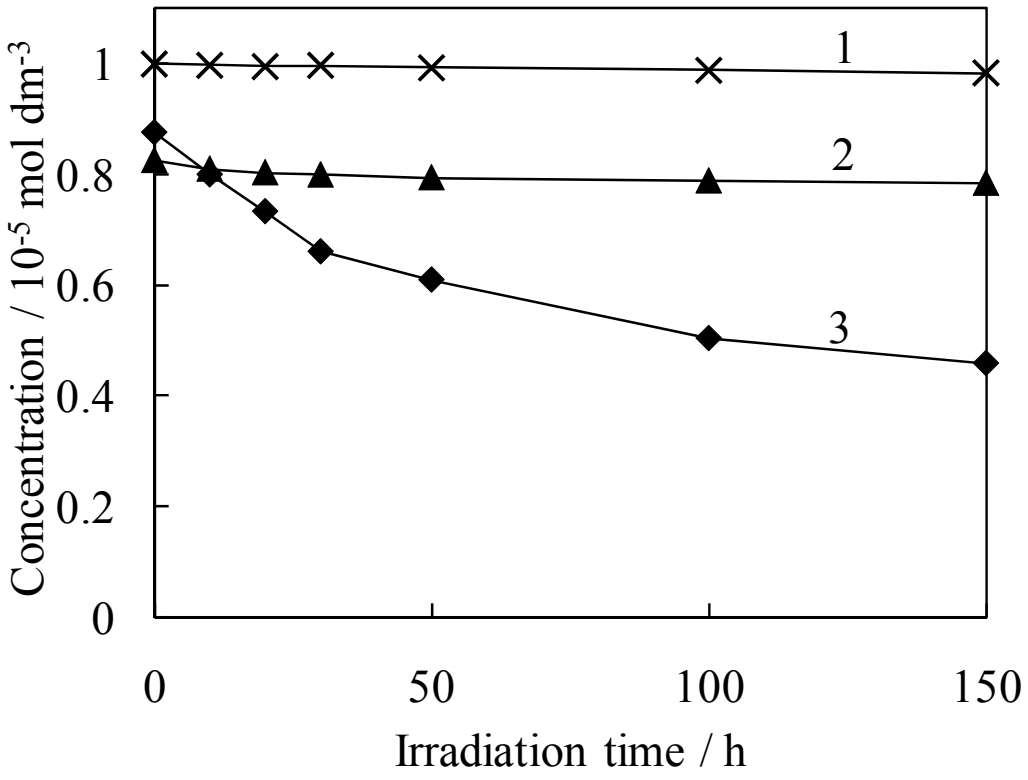
Concentration / 10-5 mol dm-3
1
0.8
0.6
0.4
0.2
0
0
50
100
150
Irradiation time / h
1
2
3

Figure 14

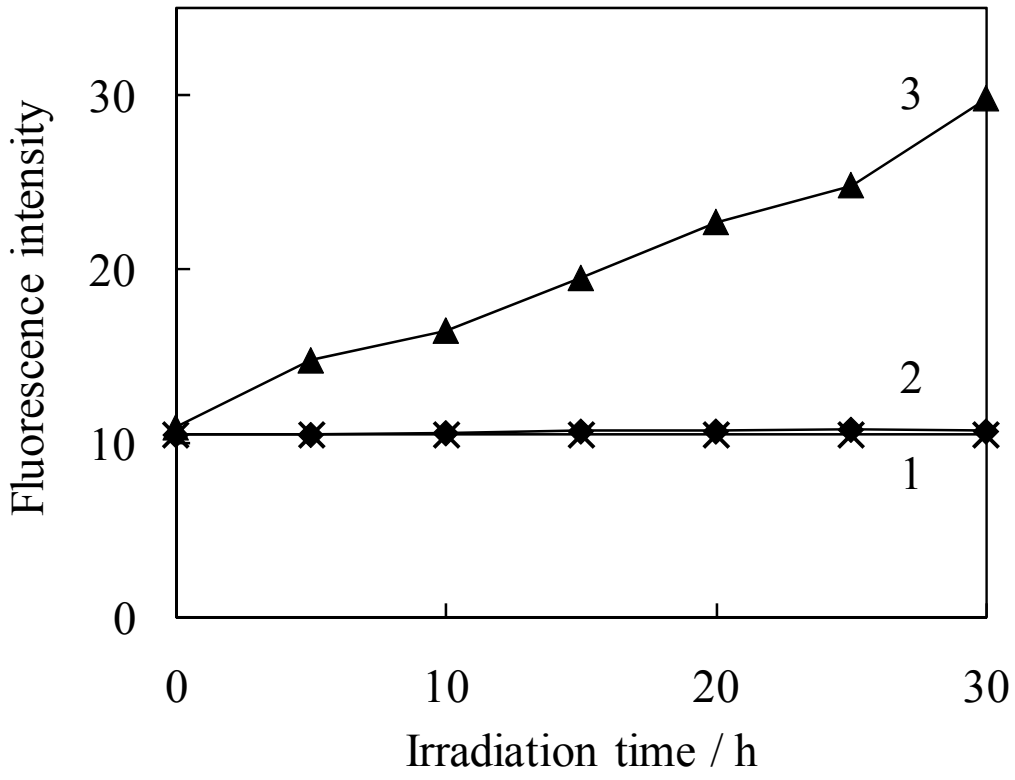
Fluorescence intensity
30
20
10
0
0
10
20
30
Irradiation time / h
3
2
1

Figure 15

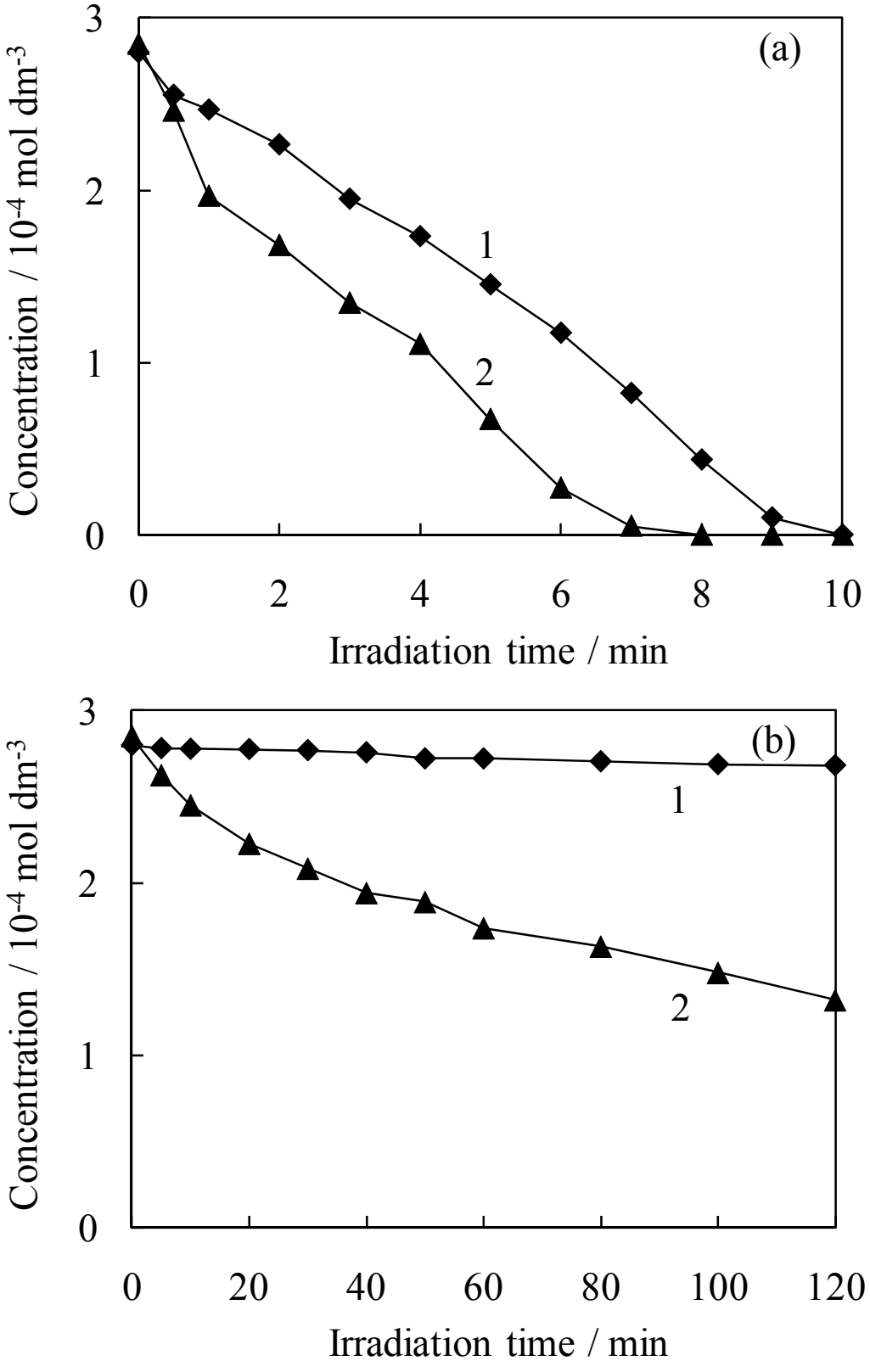
(a)
Concentration / 10-4 mol dm-3
Irradiation time / min
1
2
0
1
2
3
0
2
4
6
8
10
(b)
Concentration / 10-4 mol dm-3
Irradiation time / min
1
2
0
1
2
3
0
20
40
60
80
100
120